Journal of Cleaner Production 274 (2020) 123020

Contents lists available at ScienceDirect

Journal of Cleaner Production

journal homepage: www.elsevier.com/locate/jclepro

Alternative alkali-activator from steel-making waste for one-part alkali-activated slag

Elijah Adesanya [a, *], Katja Ohenoja [a], Andrea Di Maria [b], Paivo Kinnunen [a], Mirja Illikainen [a]

[a] Faculty of Technology, Fiber and Particle Engineering Unit, PO Box 4300, 90014, University of Oulu, Finland
[b] Sustainability Assessment of Material Life Cycle, Department of Materials Engineering (MTM), Katholieke Universiteit Leuven (KU Leuven), KasteelPark Arenberg 44, 3000 KU, Leuven, Belgium

ARTICLE INFO

Article history:
Received 5 February 2020
Received in revised form
18 June 2020
Accepted 21 June 2020
Available online 17 July 2020

Handling editor: Prof. Jiri Jaromir Klemeš

Keywords:
Blast furnace slag
Alkali activation
Cleaner production
Life cycle impact assessment
Alternative activator

ABSTRACT

In this study, the use of desulphurization dust (DeS-dust) generated as a waste material during steel-making process, as an alternative activator to commercial sodium hydroxide in ground granulated blast furnace slag (GGBFS) alkali activation is proposed. The main objective was to decrease the environmental footprint of alkali-activated materials through the reuse of industrial residues. Microsilica was added to increase the amount of soluble silica and enhance the properties of the investigated binders. The results indicate that binders from alternative activator performed better, achieving a 28 days maximum strength of 33 MPa compared to 25 MPa for the sodium hydroxide activated slag. Microsilica addition to the optimum mixes reduces the rate of efflorescence and increases the setting time. Also, microstructural studies using scanning electron microscopy (SEM), x-ray diffraction (XRD) and thermogravimetric analysis (TGA) show both samples having comparable gel formation and structure. Life cycle impact assessment shows significant savings that can be made using alternative activators over sodium hydroxide activated slag. Through the use of this waste material as alternative activator in alkali-activated binders, an environmentally friendly, and cleaner production of alkali-activated binders can be achieved having comparable or superior performance as the reference binder activated with commercial sodium hydroxide.

1. Introduction

Ordinary Portland cement (OPC) is the most used material in modern buildings construction, with a global consumption rate of 20 Gt per year (Scrivener et al., 2018). This global success of OPC-based construction materials is indubitably due to its ease of use. The OPC and aggregates are mixed with water, forming a highly functional and easily manipulable solid. On top of that, it is a low-cost material, made from some of the most available elements on earth (Pontikes and Snellings, 2014).

This technical and economic success for OPC did not come without environmental consequences. The production of OPC is indeed associated with severe environmental impacts, due to the high amount of greenhouse gases (GHG) emissions, as a consequence of (i) the calcination of limestone during clinker production, and (ii) the intensive energy production process (Maddalena et al., 2018). Globally, OPC production contributes between 5 and 8% of the total anthropogenic CO_2 emissions (Turner and Collins, 2013; van Deventer et al., 2010).

In response to the need for more sustainable alternative binders to replace OPC, different methods have been extensively studied and proposed, such as the partial substitution and blending of OPC with supplementary cementitious materials (SCM). The most common SCMs used today are fly ashes from coal burning, slags from iron-making processes, rice husk ashes, and other pozzolanic materials (Carvalho et al., 2017; Feng et al., 2004; Majhi and Nayak, 2020; Mallisa and Turuallo, 2017; Osborne, 1999). As an alternative to substitution and blending, another well-explored technologies is alkali activation, which aims to utilize alkaline industrial waste and other by-products to produce low-carbon cement materials to replace OPC (Adesanya et al., 2016; Bernal et al., 2014; Duxson et al., 2007). The industrial waste streams include fly ash, metallurgic slags and mine tailings. These streams are mixed with alkaline

* Corresponding author.
E-mail address: elijah.adesanya@oulu.fi (E. Adesanya).

https://doi.org/10.1016/j.jclepro.2020.123020

activators, such as sodium hydroxide (SH) and sodium silicate, to form a hardened matrix with comparable or superior properties than OPC. According to Duxson et al. (2007) and Habert et al. (2011), alkali-activated materials (AAMs) can lower the GHG emission by 45–80% compared to OPC, depending on the waste precursor and the alkaline activators employed in the process. Despite producing a lower amount of GHG emission, Habert et al. (2011) also showed that AAM's production may have other environmental issues such as human toxicity, freshwater and marine ecotoxicity that may compromise the final sustainability of AAMs. These footprints are derived mostly from the production of the alkaline activators. Additionally, due to their high economic costs, the commercial alkali activators represent an important economic barrier in the future development of AAMs.

Therefore, current research trends in AAMs development focuses on finding alternatives to commercially available alkaline activators with a lower environmental impact and similar or superior strength development. One promising and innovative method is to use waste precursors having high contents of alkalis that can be simply dissolved when water is added similar to one-part AAMs synthesis. One-part AAM is the dry mixing of solid aluminosilicates and solid alkali activators such as alkali hydroxides, silicates, sulfates or carbonates. Water is added in a similar mixing to OPC. While two-part AAM on the other hand is the activation of solid calcio-aluminosilicates using aqueous solutions of these alkali activators (Luukkonen et al., 2018a). This methodology (one-part) is widely suggested to achieve greater potential for large scale AAM production than the convectional two-part AAMs (Adesanya et al., 2018a; Luukkonen et al., 2018a).

Several alternatives have been studied using waste materials containing soluble alkaline sources, which can allow a reduction of up to 60% of the environmental impacts linked with the traditional alkali activators production (Mellado et al., 2014; Passuello et al., 2017). Previously, authors such as Luukkonen et al. (2018b), studied the effect of two silica sources (rice husk ash or micro silica) in combination with sodium hydroxide on blast furnace slag (GGBFS) reactivity. The study reported about 35 MPa compressive strength for both silica sources at 28 days, which makes the produced AAM suitable for some structural purposes. Other authors have investigated the potential use of other waste materials, such as maize cobs and maize stalk ashes (Peys et al., 2016), sugar cane straw ash (Moraes et al., 2018), industrial cleaning solution (Cristelo et al., 2019; Fernández-Jiménez et al., 2017), paper sludge (Adesanya et al., 2018a), Bayer process liquor (van Riessen et al., 2013), and glass waste (Puertas et al., 2015; Puertas and Torres-Carrasco, 2014; Torres-Carrasco et al., 2014). In general, all these studies obtained good properties for the hardened AAMs.

Another waste precursor that can be potentially used as an alternative to alkaline activators is desulphurization dust (DeS-dust). DeS-dust is a waste material produced during steel making processes. It is generated in the form of fine powders rich in sodium and calcium. Currently, DeS-dust is considered as waste and mostly disposed in designated landfills, with high economic costs to steel-making producers.

Hence, this paper aims to investigate the technical feasibility to use DeS-dust as an alternative alkaline activator source in place of commercial sodium hydroxide in alkali-activated GGBFS in a pathway like one-part AAMs and its environmental sustainability. Though GGBFS itself possesses hydraulic properties, increasing its environment alkalinity can further increase the rate of reaction and strength gain. Compared to other alkali activation methods, the proposed technique does not require any pretreatment with commercial alkaline activators, due to the intrinsic alkaline properties of the DeS-dust. All the materials used can be potentially sourced from the same iron and steel-making plant. First, the optimal amount of DeS-dust is investigated, and then micro silica is added to enhance the reactivity of the best mix determined by the compressive strength results. As a reference for each mix, an equivalent amount of Na_2O from commercial sodium hydroxide (SH) is used. Suitability assessment of the final blends is based on strength test, efflorescence, and setting time. The reaction kinetics is analyzed through isothermal calorimetry, and the hydration products were determined using X-ray diffraction (XRD), Scanning electron microscopy (SEM) and thermogravimetry analysis (TGA). Also, the environmental impacts of the AAMs activated by DeS-dust are investigated through a life cycle assessment (LCA), and further compared with AAMs activated by sodium hydroxide.

2. Materials and methods

2.1. Materials

The GGBFS (d_{50} = 10.8 μm) used in this investigation was obtained from Finnsementti (Finland), while the DeS-dust (d_{50} = 4.5 μm) was collected from SSAB Europe Oy (Raahe, Finland). Microsilica (MS) with tradename "Parmix-silika" was obtained from Fescon Oy (Finland) as granulated particles and was then further ground using Retsch mortar grinder RM 200 for 10 min with a d_{50} of 23 μm. MS was used as additional silica source in the binder. Their chemical compositions as analyzed through X-ray fluorescence (XRF) is presented in Table 1. The DeS-Dust contains 23.4% of sodium oxide (Na_2O) and has a pH of 13.3 which is suitable for the alkali activation of GGBFS. Standard sand conforming with EN 196-1 was used as aggregates in the mortars. Sodium hydroxide pellets (>99% pure) used as alkali activator in the reference samples was supplied by Sigma-Aldrich and deionized water was used as added water. The particle size distribution of the materials was analyzed through the laser diffraction technique (Beckman Coulter 13320) using the Fraunhofer model. Isopropanol was used as the dispersion medium to avert the reaction of particles during the measurement.

2.2. Sample preparation

In the first stage, the DeS-dust samples were prepared by blending the dry precursors for 1 min using a shear mixer (IKA Eurostar). Deionized water is then added and mixed further for 1 min. Sand is further added and mixed for another 6 min. The reference samples using commercial SH were prepared by mixing the required amount of SH with water and cooled down before use. This alkaline solution is then added to GGBFS and mixed for 1 min before sand was added and further mixed for 6 min. The water-to-binder and aggregate-to-binder ratios were kept constant at 0.45 and 2 respectively. After mixing, the samples were compacted using a jolting table, and then cast in a sealed rectangular 20 × 20 × 80 mm molds. After that, the samples are cured at room temperature (RT) and another batch at 60 °C, then demolded after 1 day and kept in a humidity chamber conditioned at 23 °C and relative humidity of 97%. The samples were then tested at 3, 28 and 60 days. The mix composition for each sample is shown in Table 2. The molar composition (Na_2O), the ratios (H_2O/Na_2O, SiO_2/Al_2O_3,

Table 1
Chemical composition in wt.% of GGBFS, DeS-dust and MS shown as oxides.

Oxides (%)	CaO	Al_2O_3	SiO_2	MgO	Fe_2O_3	Na_2O	K_2O	SO_3	LOI[a] 950 °C
GGBFS	38.5	9.5	32.3	10.2	1.23	0.5	0.5	4.0	−1.3
DeS-dust	36.8	0.4	2.6	0.7	20.9	23.4	1.8	3.7	1.2
MS	0.78	0.23	94.2	0.35	0.84	0.18	0.56	0.13	2.3

[a] Loss on ignition.

Na_2O/SiO_2, and Na_2O/Al_2O_3) for DeS-dust activated slag (i.e. DD15), and the reference SH activated slag (i.e. SH2) in Tables 2 and 3 were formulated to have similar values for comparisons.

In the second stage, the optimum content of DeS-dust in the mix composition (from Table 2) was determined based on the strength, to be for sample DD15. This was then further modified by adding various contents of MS to enhance the reactivity of the mix as shown in Table 3. The mix also was done following the procedure in the first stage.

Compressive and flexural strengths for the mortar samples were tested at 3, 28 and 60 days, using a Zwick testing instrument with a maximum loading of 100 kN. The force speed was 2.4 kN/s and 0.05 kN/s for compressive and flexural strengths respectively. To determine the efflorescence, the mortars were half-immersed in water and visually analyzed after 1 and 7 days. The reaction kinetics was measured using an isothermal calorimeter (TAM air instrument) at 23 °C. The heat of hydration was normalized using the weight of solid materials in each paste samples.

Paste samples were used for characterization analyses. The hydration of the finely ground paste samples was stopped at 3 and 28 days through the solvent exchange technique, using acetone as described in previous literatures (Adesanya et al., 2018b; Chavda et al., 2015). Thermogravimetric analysis (TGA) was done using Precisa Gravimetrics AG "prepASH automatic drying and ashing system". The samples weighted between 3 and 5 g, were heated from 30 to 1100 °C at 10 °C/min in an inert nitrogen atmosphere. The quantification of the paste mineralogy was determined through XRD, performed using Rigaku SmartLab 9 kW X-ray diffraction equipment. The analysis employed Cu Kα radiation (Kα1 = 1.78892 Å; Kα2 = 1.79278 Å; Kα1/Kα2 = 0.5), at a scan rate of 3°/min in the range 5–70° (2θ), and 0.02°/step. Phase identification was done using "X'pert HighScore Plus" (PANalytical software).

A TAM Air calorimetry instrument was used at 23 °C, to study the heat evolution in the first 80 h of reaction of the paste, according to the mix proportion in Tables 2 and 3 The samples were mixed ex-situ, hence the heat generated in the first 45 min of each mix was not used. Scanning electron microscopy (SEM) using backscattered electrons (BSE) and energy dispersive X-ray (EDS) was done for the paste samples using a Zeiss Ultra Plus (Germany), with an accelerating voltage of 15 kV. Before scanning, the samples were impregnated with epoxy resin under vacuum, and then polished using diamond pastes.

3. Results and discussion

3.1. Effect on strength development

The optimum content of DeS-dust, based on the strength at 3 days and 28 days, was determined at a ratio of 15% of DeS-dust and 85% of GGBFS, cured at RT as (see Table 4). As already demonstrated by Gebregziabiher et al. (2015), curing alkali-activated binders at elevated temperature increases reaction degree, especially at an early age. However, curing at elevated temperature had no significant effect on the strength of the samples, as the RT-cured samples exhibited higher strengths at 3 and 28 days. Hence, elevated temperature curing is not beneficial to the degree of reaction of the binders analyzed here.

Subsequently, sample DD15 and its reference SH mix (SH2) were further used with the addition of micro silica, that it is added to increase the alkalinity and RT condition used (Table 3). The addition of silica in the mix composition shows a slight improvement in the compressive strength, as reported in Fig. 1. MS2-DD15, with a 5% addition of MS, showed the highest strength at 33 MPa after 60 days, compared to neat (no MS) DD15 which shows a compressive strength of 32 MPa. The slight influence of the MS addition on the strength properties may be due to the lower dissolution rate of MS. This lower dissolution is an effect of the MS particle size (d50 = 23 μm), the unreacted MS subsequently acting as a filler in the binder. At 60 days, MS1-DD15 showed no increment in strength but had similar strength (within the error bar) of the strength at 28 days.

On the other hand, the addition of MS to the commercial SH activated GGBFS showed no significant influence on the compressive strength, regardless of the curing age analyzed (Fig. 1b). The strength recorded for these samples is comparable with results from previous studies, such as Luukkonen et al. (2018b), which used a comparable mix composition.

Overall, GGBFS mortars activated by DeS-dust exhibited superior compressive strength than the refernce commercial SH activated GGBFS mortars. This can be partially attributed to the additional dissolution of other elements (i.e. Ca and Fe) in the DeS-dust contributing to the hardened properties of the DD15 activated mortars. To support this hypothesis, the beneficial role of iron (Fe) in alkali-activated materials synthesis have been already documented in previous studies (Adesanya et al., 2020; Lemougna et al., 2013; Onisei et al., 2018; Simon et al., 2018). Overall, the Ca and Fe content in the DeS-dust containing mortars are higher than in SH mortars and could have influenced the higher strength, since the sodium oxide composition of these mixes were kept constant.

3.2. Reaction kinetics and setting time

The generated heat flow (J/h·g) and the total heat released (J/g) from the binders, normalized to the solid content weight, are shown in Fig. 2. The evaluation of the heat flow profiles shows similarities to the one of OPC, though the chemical activity is significantly different (Gebregziabiher et al., 2015; Qu et al., 2016; Sun and Vollpracht, 2018). Hence, similar descriptions can be used

Table 2
Mix composition in wt.% of each sample (first stage).

Sample name	Fraction of binders in wt.%				Na_2O[a]	Molar ratios			
	DeS-dust	GGBFS	SH	MS		H_2O/Na_2O	SiO_2/Al_2O_3	Na_2O/SiO_2	Na_2O/Al_2O_3
DD10	10	90	–	–	0.09	55.30	5.74	0.09	0.53
DD15	15	85	–	–	0.13	39.30	5.75	0.13	0.80
DD20	20	80	–	–	0.16	30.40	5.76	0.18	1.01
DD25	25	75	–	–	0.20	24.90	5.78	0.24	1.40
DD30	30	70	–	–	0.24	21.00	5.79	0.30	1.80
SH1	–	98	2	–	0.09	53.30	5.72	0.08	0.51
SH2	–	97	3	–	0.13	39.30	5.72	0.12	0.70
SH3	–	96	4	–	0.16	30.50	5.72	0.16	0.92
SH4	–	95	5	–	0.20	24.90	5.72	0.20	1.13
SH5	–	94	6	–	0.24	21.00	5.72	0.24	1.40

[a] Na_2O molar composition in each mix.

Table 3
Mix composition in wt.% of each sample modified based on DD15 composition (second stage).

Sample name	Fraction of binders in wt.%				Na_2O[a]	Molar ratios			
	DeS-dust	GGBFS	SH	MS		H_2O/Na_2O	SiO_2/Al_2O_3	Na_2O/SiO_2	Na_2O/Al_2O_3
MS1-DD15	15	82	–	3	0.13	39.40	6.36	0.13	0.82
MS2-DD15	15	80	–	5	0.13	39.50	6.79	0.12	0.84
MS3-DD15	15	77	–	8	0.13	39.50	7.36	0.11	0.86
MS1-SH2	–	94	3	3	0.13	39.10	6.25	0.12	0.72
MS2-SH2	–	92	3	5	0.13	39.10	6.62	0.12	0.74
MS3-SH2	–	90	3	8	0.13	39.20	7.11	0.11	0.76

[a] Na_2O molar composition in each mix.

Table 4
Compressive strengths of mortars in the preliminary investigations.

Sample name	Room temp. (23 °C)		Cured at 60 °C	
	3 days (MPa)	28 days (MPa)	3 days (MPa)	28 days (MPa)
DD10	15 ± 0.4	28 ± 3.0	14 ± 0.2	17 ± 0.7
DD15	17 ± 0.5	29 ± 0.7	13 ± 0.4	18 ± 0.7
DD20	15 ± 0.7	25 ± 2.0	14 ± 0.3	17 ± 1.9
DD25	14 ± 0.9	24 ± 1.2	16 ± 1.2	21 ± 3.1
DD30	14 ± 0.3	21 ± 1.4	14 ± 0.7	17 ± 1.0
SH1	14 ± 0.5	28 ± 2.3	13 ± 0.5	16 ± 0.7
SH2	13 ± 0.5	25 ± 1.4	12 ± 0.6	13 ± 1.2
SH3	14 ± 0.5	25 ± 2.0	13 ± 1.1	17 ± 0.4
SH4	12 ± 0.9	22 ± 1.3	12 ± 0.5	14 ± 1.2
SH5	15 ± 0.9	22 ± 1.3	13 ± 0.5	16 ± 0.9

to label the reaction stages. It should be noted that the heat flow data for the first 45 min was not used due to the waiting period for equilibration of the calorimeter after samples are inserted.

The first peak seen during the first 2 h reaction is attributed to the heat released from wetting and dissolution, occurring when water is added to the binder. This initial exothermic peak is significant with paste activated using DeS-dust, and may define the material degree of dissolution over SH. The second intense peaks after the very short induction period correlates with the acceleration-deceleration period associated with precipitation of reaction products in the paste (Nguyen et al., 2019; Shi and Day, 1995). The condensation and formation of reaction products are exothermic and contributed to this intense peak. The magnitude of these peaks is significantly modified by the addition of micro silica (3–8%) when compared with DD15 and SH2.

Increasing the silica content with MS slightly broadens the heat released peaks, and increases the cumulative heat released. Furthermore, no noteworthy peaks were observed after the second peak, as the heat of reaction decelerates slowly. After 80 h reaction, DeS-dust activated slag samples recorded a higher cumulative heat release at approximately 230 J/g, and 180 J/g for SH-activated slag samples.

Also, the initial setting time of the binders was determined. The initial setting time is an important parameter because it controls the mixing, handling, transportation and casting of the matrix. Mix proportions similar to the one of the mortar samples were used, except for the use of aggregates. The test results (Fig. 3) showed that DD15 has the most rapid initial setting time, losing its plasticity at 60 min. SH2 initial setting time was recorded to be 170 min. DD15 setting performance is comparable with the setting of other one-part alkali-activated materials, because of the heat generated from the fast dissolution of alkali hydroxides in the binder (Luukkonen et al., 2018a; Suwan and Fan, 2017). This is finally consistent with the higher heat flow of DD15 than SH2 observed in Fig. 2.

Recommended initial setting time should be between 45 and 75 min, depending on the strength class (EN 197-1, 2011),.

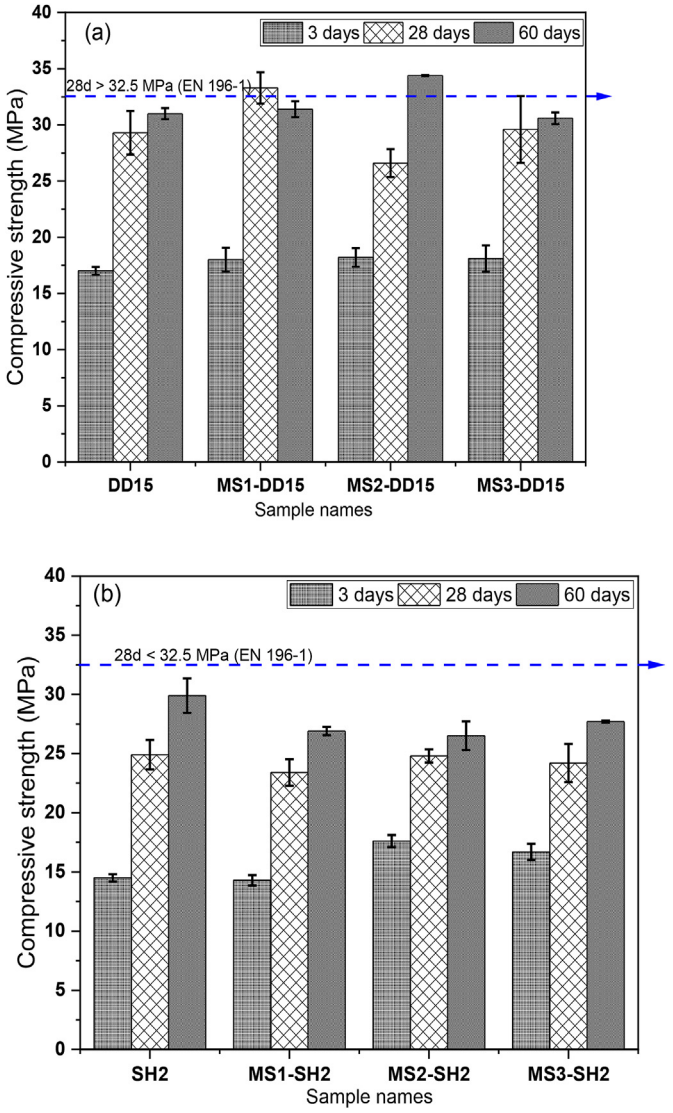

Fig. 1. Effect of microsilica addition on the compressive strength of GGBFS activated with (a) desulphurization dust and (b) commercial SH at 3, 28 and 60 days of curing.

However, the initial setting time was further prolonged with the addition of MS into the mix. Furthermore, the addition of 3–8% MS in the alternatively activated slag significantly increased the initial setting time. This may be attributed to the dilution effect of MS in addition to the mix. The increased initial setting time due to MS addition in GGBFS is also reported in Luukkonen et al. (2018b).

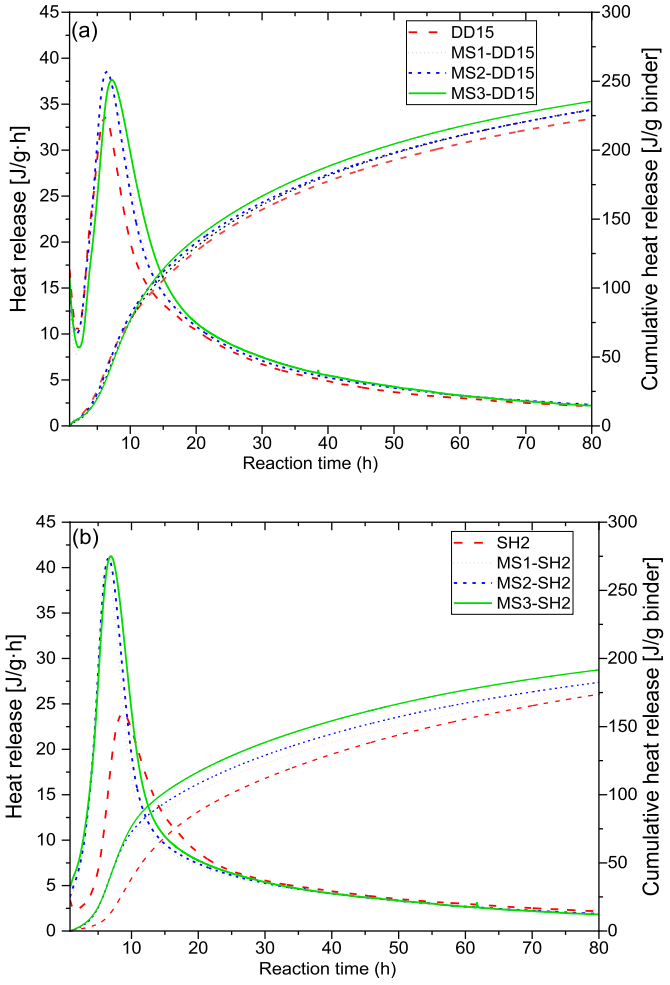

Fig. 2. Calorimetry curves showing heat released and cumulative heat released for (a) DD15-alternative activated slag and (b) SH2-activated slag after 80 h of reaction.

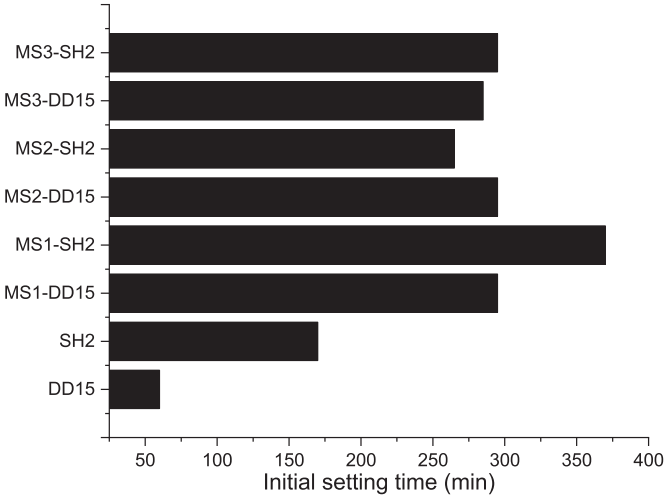

Fig. 3. Initial setting times of alkali-activated GGBFS using alternative activator (DD) and commercial activator (SH). The initial setting time is dependent on the content of MS.

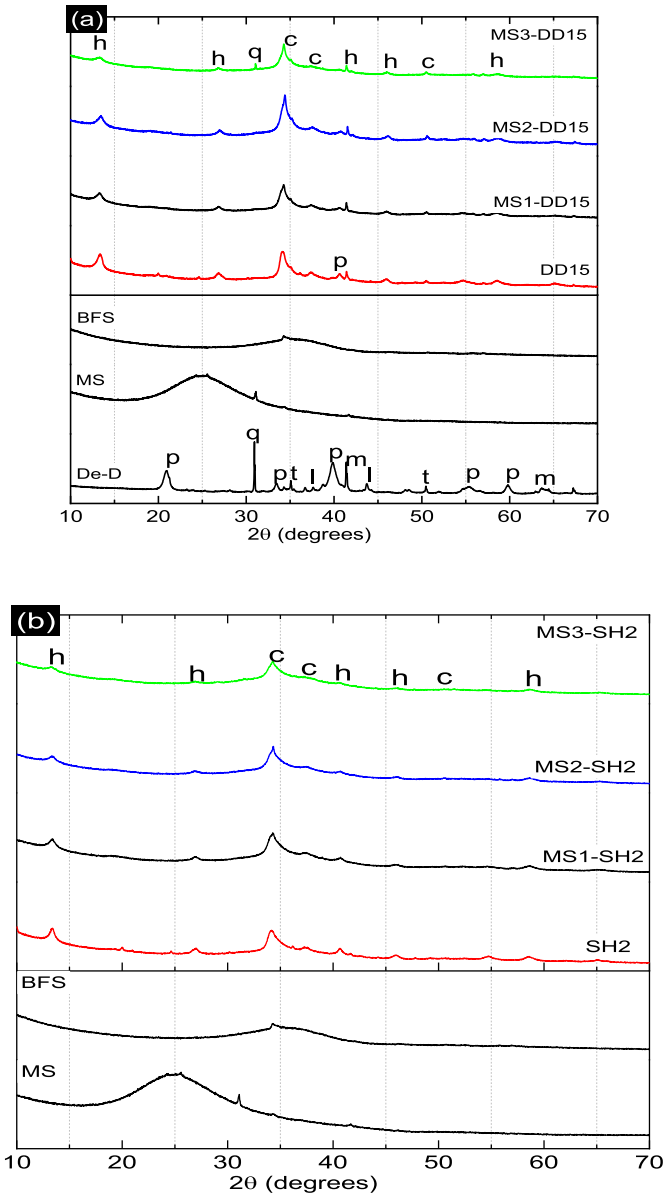

Fig. 4. XRD patterns for hardened GGBFS activated with (a) DeS-dust and (b) SH analyzed at 28 days. (p = portlandite/$Ca(OH)_2$, h = hydrotalcite/$Mg_6Al_2CO_3(OH)_{16}$, q = quartz/SiO_2, c = $CaCO_3$ or C–S–H like phase, m = magnetite/Fe_3O_4, l = lime/CaO and t = trolite/FeS).

3.3. Characterization of reaction products using XRD, TGA, and SEM

The XRD for both GGBFS and MS exhibits predominant amorphous content, whereas DeS-dust contained some major crystalline contents, such as portlandite ($Ca(OH)_2$), lime (CaO), troilite (FeS), magnetite (Fe_2O_4) and some traces of quartz (SiO_2) as seen in Fig. 4. Furthermore, the XRD of the activated GGBFS using both DeS-dust and SH exhibited the same patterns, having similar reaction products, such as hydrotalcite ($Mg_6Al_2CO_3(OH)_{16}.4H_2O$) and C–S–H like-phase diffraction pattern. These reaction product peaks are consistent and correlated to previous studies on GGBFS alkali activation (Adesanya et al., 2018a; Ben Haha et al., 2012; Luukkonen et al., 2018b). The C–S–H like-phase overlaps with another identified peak of calcite ($CaCO_3$), which may have been present as a result of carbonation during sample curing or XRD preparation.

The TGA/DTG of the samples shown in Fig. 5 further confirms

the reaction product of the activated GGBFS. The first weight loss at 60–230 °C indicates the dehydration and presence of C–S–H-like solid (C-A-S-H and/or C-(N)-A-S-H) in the paste (Abdel Gawwad et al., 2016; Ben Haha et al., 2012; Rashad et al., 2012). Compared with SH2-activated GGBFS, this peak was clearer for DeS-dust activated GGBFS, and it may suggest dehydration of a higher amount of the reaction product formed in the paste, due to higher Ca content in the system. The shoulder around 230 °C and the peaks at 400 °C is consistent with the weight loss of hydrotalcite-like solid phases (M. Ben Haha et al., 2011; Collier, 2016). The peaks between the temperature range of 520–750 °C are explained by the decarbonation of calcite in the paste identified in the XRD of these samples. The decarbonation peak for DD15 was more intense than the peaks of the other sample containing MS. This can be attributed to the decrease in CaO content when MS is added and the amount of carbonatable constituent is decreased. The effect of increased silica addition in the degree of carbonation in the cement paste is also in previous studies (Papadakis, 2000; Zhang and Li, 2013).

The BSE-SEM images in Fig. 6 reveals the microstructure of DD15 and MS2-DD15 after 28 days. The presence of partially reacted slags (light gray particles) and reaction products (dark gray), distinguished by different gray levels, associated with variation in average atomic density (Humad et al., 2019). Furthermore, it is also possible to observe some partially dissolved whitish particles on the DD15 samples (Fig. 6a), which is attributed to the ferrite phases in the DeS-dust. The partially reacted slag particles is seen surrounded by rims. These rims are characteristically C–S–H gel according to EDX spectra (data not shown). Similar observations have been reported in (M. M Ben Haha et al., 2011).

Some microcracks in the binders are also present, which may have formed during the specimens cutting and polishing. Compared with DD15, the effect of MS addition on the microstructure of MS2-DD15 shows a denser structure of the product gel areas. The SiO_2–CaO–Al_2O_3 ternary diagram in Fig. 6c and (d) shows the plot of EDX spectrum points of the BSE-SEM images, reported in Fig. 6a and (b) (excluding unreacted precursors). For the EDX calculation, the atomic ratios were normalized to the content of Al_2O_3, SiO_2 and CaO, neglecting other oxides. The data plots show the variation in the gel's oxides composition. The black circled areas indicate the probable region of a C-A-S-H and N-A-S-H type gel (or a C-(N)-A-S-H type gel), the dotted blue circle corresponds to C-A-S-H type gel formation region, and the red dashed circle corresponds to an N-A-S-H type gel (Garcia-Lodeiro et al., 2011; Humad et al., 2019; Ismail et al., 2014). Fig. 6c shows clustered and scattered regions of points corresponding to a C-A-S-H and C-(N)-A-S-H type gels formation in the binder (Garcia-Lodeiro et al., 2011). The Ca/Si ratio in this region is between 0.78 and 3.78 and Al/Si ratio between 0.0 and 0.80. In Fig, 6 d, the Ca/Si ratio of the points in the plot ranges between 0.45 and 2.52 and Al/Si ratio between 0.08 and 0.42. The differences related to these ratios can be explained by the influence of MS addition into the paste. The addition of this silica source contributes to the reaction products.

3.4. Effects of silica addition on efflorescence of mortars

The rate of efflorescence in the mortar is dependent on the amount of MS added to the mortar mix. Fig. 7 shows the degree of efflorescence after 7 days. The whitish crystals began appearing after 3 days of analysis. Efflorescence in AAMs is derived through the reaction of available OH^- and soluble alkali metals (i.e. Na^+) in the specimen with atmospheric CO_2 to form whitish alkali carbonates which are deposited on the specimen, the formation is outlined below (Zhang et al., 2014):

$$CO_{2\,(g)} + 2OH^-_{\,(aq)} \rightarrow CO_3^{2-}{}_{(aq)} + H_2O \quad (1)$$

$$2Na^+_{\,(aq)} + CO_3^{2-}{}_{(aq)} + nH_2O \rightarrow Na_2CO_3 \cdot nH_2O_{\,(s)} \quad (2)$$

The whitish crystals were collected and analyzed through XRD: alkali carbonates (trona and thermonatrite) were mainly identified as the mineral phase (see Fig. 8). It is recognized that efflorescence in AAMs is dependent on the microstructure pores acting as a leaching conduit, where the ions are leached out to the surface of the mortar (Zhang et al., 2014, 2014, 2013). The effect of MS addition on the reduction of efflorescence can be deducted partially as the physical compaction and the filling of open pores by unreacted MS in the specimen, stopping the leaching channels. Increasing MS content in the binder may have resulted in more unreacted MS which are available to fill open pores. This assumption and effect of MS on the specimen are in agreement with experimental observation with some previous studies (Wang et al., 2018; Zhang and Li, 2013) and the results of carbonation from TGA/DTG.

3.5. Life cycle assessment

Together with sound technical characteristics, a sustainable environmental profile is another fundamental prerequisite for the successful development of new technologies on an industrial scale. Therefore, in this last chapter, the environmental profile of DeS-

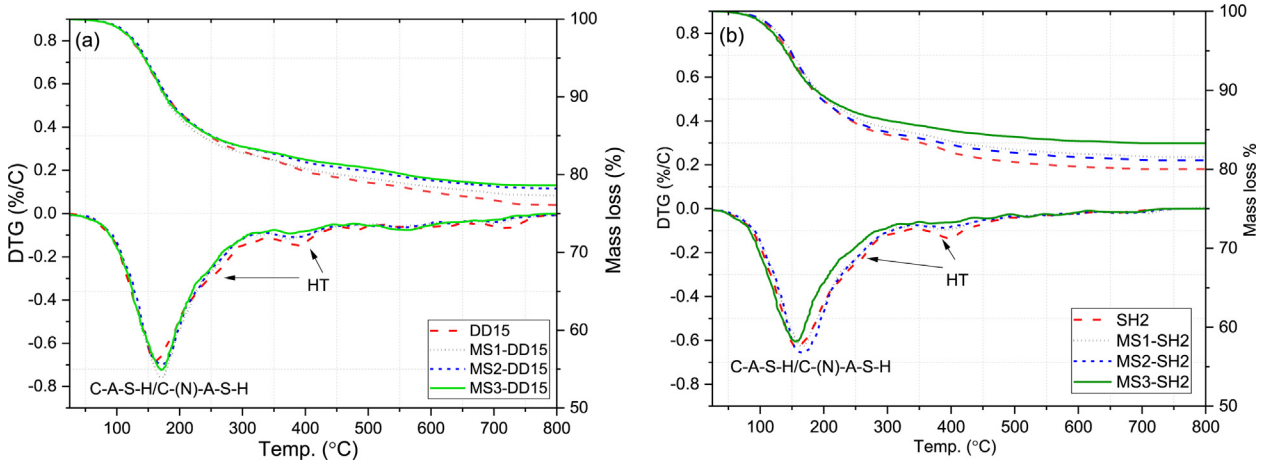

Fig. 5. TGA/DTG curves of the powdered GGBFS activated paste with (a) DeS-dust and (b) SH analyzed at 28 days.

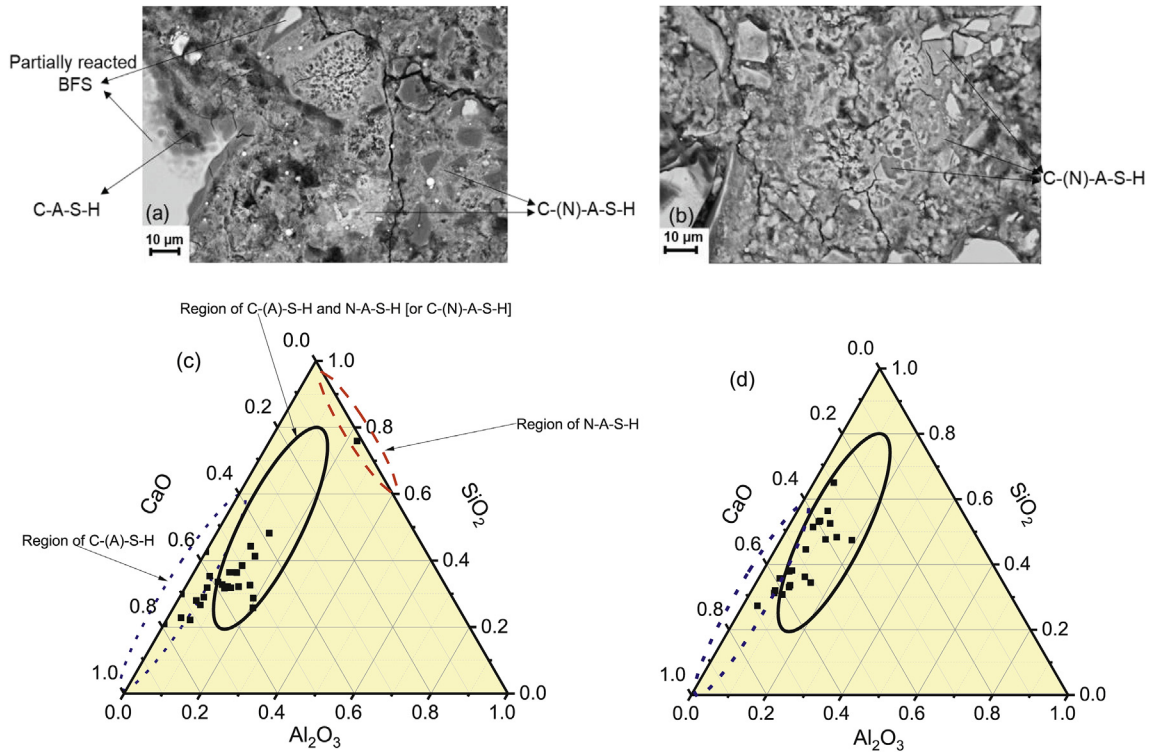

Fig. 6. BSE-SEM images showing the microstructure of the binder after alkali activation (a) DD15 (b) MS2-DD15 and the equivalent ternary diagram plots of the reaction products oxides (c) DD15 and (d) MS2-DD15.

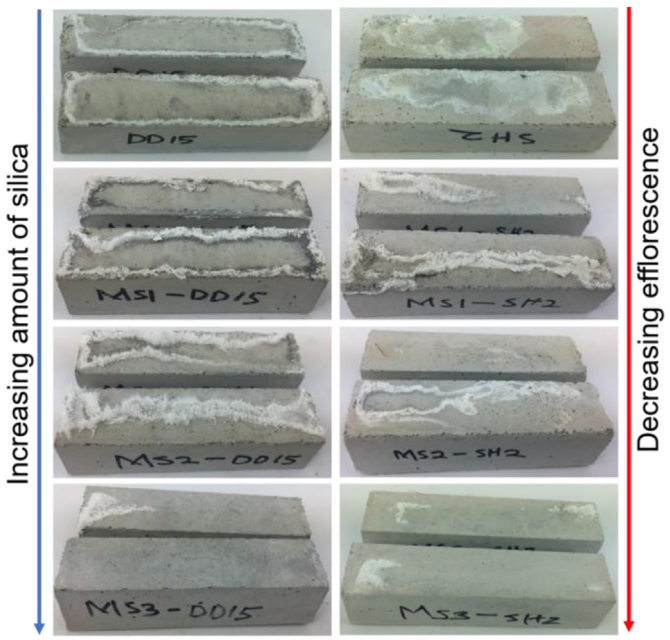

Fig. 7. Efflorescence of mortar samples of 28 days-aged alkali-activated GGBFS half immersed in water for 7 days.

dust based mortar is evaluated and compared with the environmental profile of (i) AAMs mortar activated with sodium hydroxide and (ii) traditional OPC mortar. Life cycle assessment (LCA) is used as a methodology to calculate the environmental impacts due to the production of the compared materials. The general LCA-framework is described by the ISO 14040:2006 (ISO 14040, 2006,

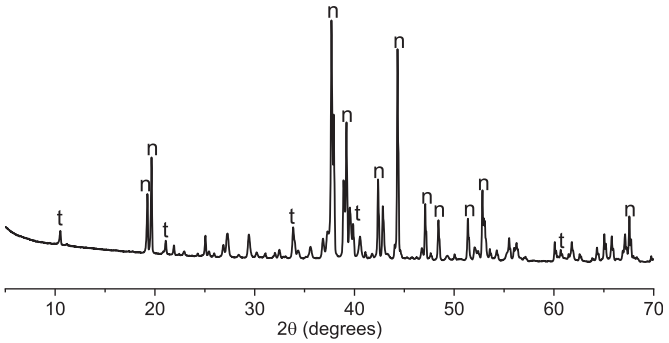

Fig. 8. XRD pattern of the efflorescence residues on the mortar (n = thermonatrite [$Na_2(CO_3)(H_2O)$] and t = trona [$HNa_3(CO_3)_2(H_2O)_2$]).

p. 14040), and it consists of four phases: defining the goal and the system boundaries, creating a life-cycle inventory, assessing the impacts, and interpreting and analyzing the results.

In the following subsections, the LCA study, comparing DeS-dust, sodium hydroxide AAMs and OPC mortars, is performed following the four phases indicated by the ISO 14040.

3.5.1. Goal and functional unit of the environmental analysis

The goal of the LCA presented in this chapter is to compare the environmental performances of DeS-dust based mortar with sodium hydroxide AAMs mortar and traditional OPC mortar.

The first step of LCA is the definition of the functional unit (FU) and the system boundaries of the analysis. The FU provides a reference to which all quantities must be referred, and it expresses the product's ability to perform a pre-defined function. When comparing the LCA of products with different characteristics, the FU must ensure a fair comparison.

Mortars are used as an intermediate product in the production of construction blocks. As discussed by previous LCA studies comparing different binders, a comparison based simply on mass (1 kg of alkali-activated mortars vs 1 kg of OPC mortar) is not correct, since the different amount of each mortar is required to produce construction blocks with similar characteristics (Di Maria et al., 2018; Habert et al., 2011). To ensure a fair comparison between the different mortars, the selected FU of the LCA refers to the capacity of the mortar to resist against an axial compressive force per unit surface. This capacity is commonly known as compressive strength and it is expressed in MPa (N/mm^2). More specifically, all calculations in the LCA refers to the amount for each mortar able to provide a compressive strength of ≈30 MPa.

3.5.2. Inventory analysis and system boundaries

The inventory analysis calculates all the mass and energy inputs and outputs, concerning the FU. The studied system does not include every stage of the materials life cycle, but it only focuses on the production phase. In LCA, this is defined as the "cradle to gate" approach. This approach is justified when the analyzed product is used as an intermediate product for other applications, such as mortars used for further production of concrete. Although incomplete, this approach can already provide useful information for further construction of complete life cycles for the end-product. The cradle to gate approach implicitly hypothesizes that the use phase and end-of-life phase of the materials are similar: when cast in the structure, the impacts for the rest of the life cycle (maintenance and disposal) for AAMs geopolymers and OPC-based concretes are analogous, since they can all be considered as inert material. This hypothesis strongly depends on the durability. Although the durability of OPC concrete has been extensively investigated in the past decades, studies on the durability of AAMs geopolymer concrete are less abundant. Up to now, previous investigations on the durability of concrete structures showed a similar comportment for AAMs geopolymers and OPC concretes (Habert et al., 2011), which justify the cradle to gate approach of the presented LCA.

The system boundaries of the analysis and all inventory data used are summarized in Fig. 9. The DD15 and its reference SH mix (SH2) have been selected for the analysis, since DD15 is the mix showing the most promising characteristics in terms of strength without the use of MS. Samples with MS are not analyzed as MS used here is optional.

The difference between DD15 and SH2 lays on the amount of GGBFS and mix sand use, and on the substitution of NaOH (in SH2) with DeS-dust in DD15.

From Fig. 9, GGBFS and DeS-dust are two residues produced from an industrial process (iron and steel-making production), that are not included in the system boundaries of the analysis. Therefore, the question is then how to allocate the environmental impacts of the steel making process between the iron and steel (main products) and the GGBFS and DeS-dust (residues). The allocation issue for the use of industrial residues to produce new material is an ongoing discussion in LCA, see for instance Schrijvers et al. (2016). The ISO 14041, which defines the standards for goal and scope and inventory analysis in LCA, the allocation should be applied only when a waste can be considered as a by-product, while no allocation is advised if the waste is considered as an unintended residue.

Early LCA studies on the use of GGBFS and fly ashes as supplementary cementitious materials, solved the allocation issue by not attributing any environmental impact to these industrial residues (Van den Heede and De Belie, 2010). Other studies (Chen et al., 2010; Habert, 2013), proposed alternative allocation methods for GGBFS based on physical and economic empirical coefficients. For the LCA presented in this current study, a deep discussion of whether an allocation coefficient should be applied to GGBFS and DeS-dust goes beyond the scope of the study. Therefore, this paper follows the recommendation put forth in the ISO 14040, and no impacts are allocated to GGBFS and DeS-dust.

Consequently, the differences between DD15 and SH2 are represented by the sodium hydroxide (0.07 kg) used for SH2 production, and by the extra amount of sand (0.04 kg) that is used for DD15, compared to SH2 production. Ecoinvent 3.5 is used as a database to model the physical flows (materials and energy) used to produce the sodium hydroxide and the mixed sand.

The traditional OPC mortar mix for the required compressive strength of ≈30 MPa and a liquid-cement ratio of 0.5 can be approximated using the BRMCA mic design method (Newman and Choo, 2003). The considered OPC mortar has a design mix of 0.28 kg of cement CEM I, 0.49 kg of sand, and 0.14 kg of water, for a total weight of 0.91 kg. Although today the use of CEM II or CEM III is becoming dominant, and CEM I is no longer the most used cement type, the selection of CEM I as traditional OPC mortar in the LCA study allows avoiding allocation issues, that go beyond the scope of the paper. As already discussed above, and well explained also by Van den Heede and De Belie (Van den Heede and De Belie, 2012), allocation assumes particular relevance in the case of CEM II and CEM III, and further research should be done on proper methodologies to consider the environmental impacts to be attributed to fly ashes and BFS. The limitation of the LCA results when selecting CEM I rather than CEM II or CEM III will be further analyzed in the result discussion section.

3.5.3. Life cycle impact assessment

The life cycle impact assessment (LCIA) translates the physical flows identified during the inventory into environmental impact categories. In practice, the purpose of the LCIA is to calculate the contribution of materials and energy flows (identified during the LCI) to specific indicators with a clear environmental meaning, such as climate change or water and resources depletion (the environmental impact categories) (Bjørn et al., 2018). The selection of which impact categories are to be included in the study depends on the LCIA calculation method adopted. Several LCIA calculation methods have been published in the last decades, and any further explanation on the differences between LCIA calculation methods goes beyond the scope of this chapter. A detailed description of the science behind the LCIA phase can be found in recently published literature (Rosenbaum et al., 2018).

For the present study, the Recipe methodology is selected as the LCIA calculation method, as Recipe is one of the most commonly used methods by LCA practitioners when studying waste recycling processes (Belboom et al., 2013).

3.5.4. LCA results discussion

The results of the environmental analysis for the comparison of DD15 vs SH2 are shown in Fig. 10 and reported in Table A in the annex.

As already discussed above, the difference between DD15 and SH2 is represented by the use of sodium hydroxide (0.07 kg) in SH2 production, and an extra amount of mix sand (0.04 kg) required during the production of DD15. Therefore, for all environmental categories considered, the production of SH2 has a much higher impact than the production of DD15, since the significant difference between the environmental impact of sodium hydroxide production vs additional sand extraction.

In Fig. 10, the result of DD15 for each category is normalized to the total result for SH2, meaning that the result for SH2 is assumed to be 100%, and the value for DD15 is calculated as in percentage. The normalization allows us to represent all environmental

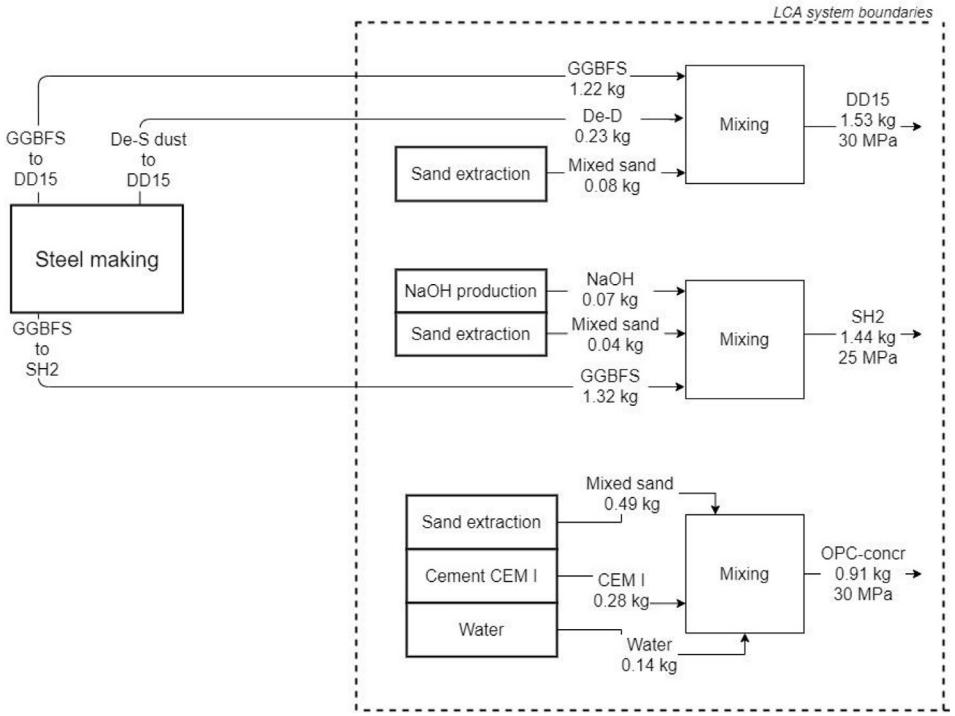

Fig. 9. *Schematic description showing the system boundaries of the analysis.*

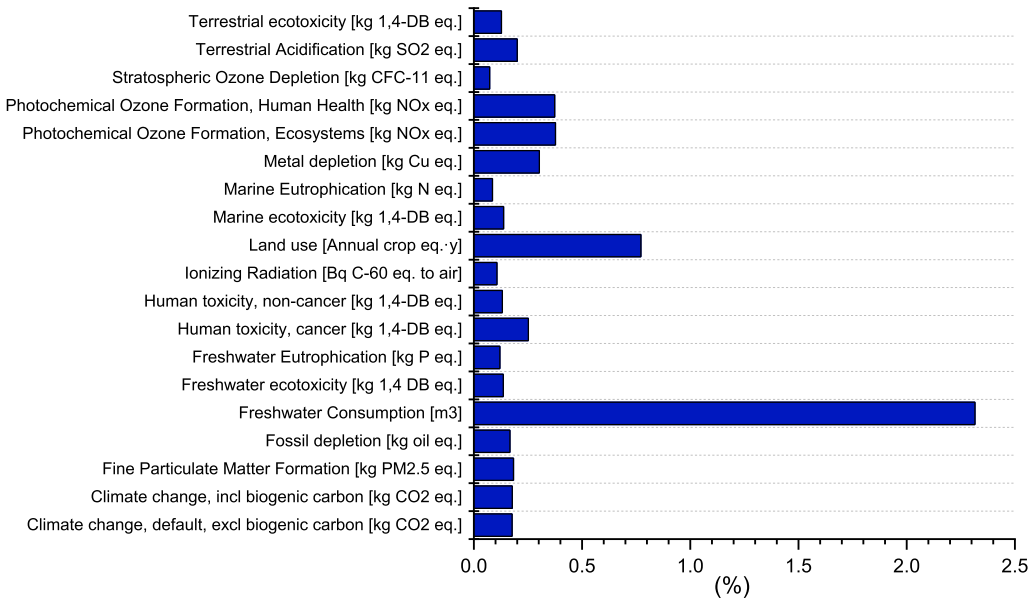

Fig. 10. Comparison of DD15 impacts as a % of SH2 environmental impacts.

categories in the same graph, as each midpoint category is measured with a different unit (see Table A in annex).

For almost all categories, the impact for DD15 is always below 1% of the impact for SH2, meaning a reduction of more than 99%. The only category where the impact of DD15 is above 1% is the freshwater consumption, with only 2.3%. Previous LCA studies on alkali-activated materials have shown how the sodium hydroxide production represents the highest contribution to the total environmental impact of the alkali activation technology (Di Maria et al., 2018; Salman et al., 2016). Therefore, the result of the LCA presented in this study show that the use of DeS-dust represents an interesting opportunity to significantly reduce the environmental impacts of alkali-activated material.

The LCA results for the DD15 and SH2 is further compared with the LCA results of traditional OPC mortar presenting the same compressive strength. Fig. 11 presents a graphical representation of the differences in the environmental impacts for DD15, SH2, OPC mortars production. Setting at the value 1 the impacts for OPC mortar in each of the impact categories, the blue columns represent the relative impact of SH2, while the orange columns represent the relative impacts of DD15 (the absolute values for OPC mortar are reported in Table A in the annex).

When compared to OPC mortar, SH2 presents a significant reduction in some of the environmental categories, indicated in Fig. 10 by the columns with a value lower than. The highest reductions are reported for the categories metal depletion (−73%) and climate change, both including and excluding biogenic carbon (−63%). However, for other categories, the environmental impact of SH2 is higher than the one of OPC mortar, represented in Fig. 11 by the dash lines with a value higher than 1. On the other hand, the impact reduction for the DeS-dust activated DD15 is ≈ 99% for all considered categories. The values for DD15 which are unseen in the graph are also shown in tabular form in Annex B. These results are easily understandable when considering that from the production of sodium hydroxide derives almost all the totality of environmental impacts of alkali-activated binders, as already demonstrated by previous literature (Di Maria et al., 2018).

The presented LCA results show the clear advantage of replacing sodium hydroxide with DeS-dust, when comparing the environmental impacts of DeS-dust active materials versus sodium hydroxide activated material and traditional OPC mortar. On the other hand, the presented results are affected by the assumption that no impact is allocated to GGBFS and DeS-dust used in the AAMs, since they are considered today as waste streams. With the further development of the alkali activation technology, the demand for these waste streams (as well as other metallurgic slags) is expected to rise, and, therefore, further research on allocation procedure will be needed. An equivalent allocation issue is also affecting the choice of CEM I as the traditional OPC mortar to be compared in the LCA, since a comparison of DD15 and SH2 with CEM II/III based OPC mortar would appear more appropriate. However, the use of fly ashes and BFS in CEM II and CEM III would have led to further allocation issues. Therefore, LCA results comparing alkali activated materials (DD15 and SH2) with traditional OPC mortar must be analyzed always keeping in mind the current limitations of LCA models in properly allocate environmental impacts for industrial residues.

4. Conclusion

In this study, the use of desulphurization dust generated from steel-making processes as an alternative activator in alkali-activated binder was investigated for the first time. The sodium-rich residue is evaluated as an alternative alkaline activator in place of sodium hydroxide in blast furnace slag ternary mix; microsilica was added to increase the soluble silica content of the mix. The AAM binders produced using just desulphurization dust and BFS exhibited a high strength of 29 Megapascal (MPa) after 28 days compared to 25 MPa for the NaOH reference binder. The addition of microsilica enhanced the strength gain to 33 MPa for the alternative activated BFS mortar suitable for EN 196-1 specifications, increased the initial setting time and reduced the occurrence of efflorescence in the mortar. Analyzed reaction products of the binders also showed similar chemistry in these different mixtures: SEM-EDX showed reaction products as calcium aluminate silicate hydrate (C-A-S-H), sodium aluminate silicate hydrate (N-A-S-H) gel type and a hybrid mix of these products (C-(N)-A-S-H). Hydrotalcite was also detected as one of the reaction products through XRD.

Overall, the LCA analysis showed significant environmental impacts that can be avoided (including landfilling) using desulphurization dust as an alternative activator in alkali-activated binders. More specifically, the LCA results show the clear environmental benefits when replacing sodium hydroxide with DeS-dust in the production of alkali-activated materials. The use of sodium hydroxide represents the main environmental hotspot of the alkali activation technology, and one of the main barriers in the development of the success of alkali-activated materials. Therefore, the presented LCA result is an important indication for further research, and it can help alkali activation to take another step towards industrial and public acceptance.

All the materials used in the synthesis except microsilica can be source from iron and steel-making plants. Also, it is proposed that desulphurization dust can be used as supplementary material with commercial blast furnace slag to induce its hydraulicity faster. To achieve a higher strength, it is suggested to decrease the particle size of microsilica below 10 μm. The alkali activated slag designed in this study can be used in structural applications, interlocking blocks and in structural repairs.

CRediT authorship contribution statement

Elijah Adesanya: Conceptualization, Methodology, Investigation, Formal analysis, Writing - original draft. **Katja Ohenoja:**

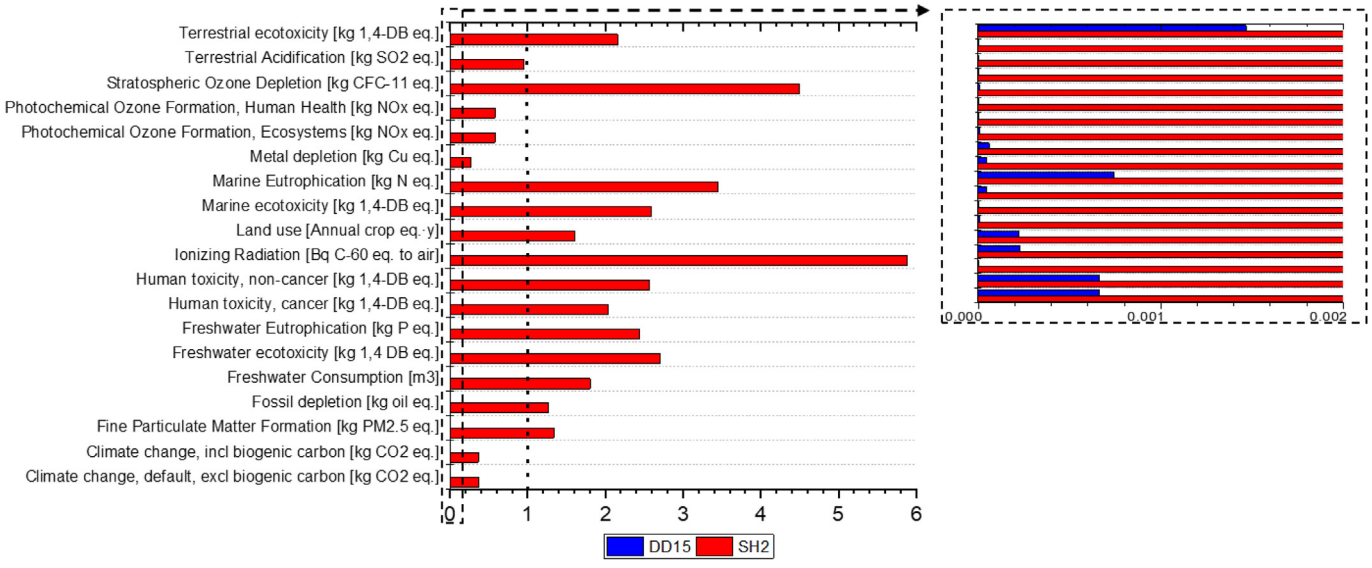

Fig. 11. Comparison of SH2, DD15 environmental impacts related to the environmental impacts of OPC mortar (set at value 1).

Conceptualization, Methodology, Supervision, Resources, Funding acquisition, Project administration, Writing - review & editing. **Andrea Di Maria:** Methodology, Investigation, Writing - original draft, Writing - review & editing, Resources, Formal analysis, Validation. **Paivo Kinnunen:** Supervision, Resources, Funding acquisition, Project administration, Writing - review & editing. **Mirja Illikainen:** Supervision, Resources, Funding acquisition, Project administration, Writing - review & editing.

Declaration of competing interest

The authors declare that they have no known competing financial interests or personal relationships that could have appeared to influence the work reported in this paper.

Acknowledgment

This work was done as a part of SYMMET project supported by the Business Finland and several Finnish companies: Boliden Harjavalta Oy, Boliden Kokkola Oy, Luxmet Oy, Outokumpu Stainless Oy, Outotec, Owatec Oy, SSAB Europe Oy, Tapojärvi Oy, and Timegate Instruments Oy. P.K. acknowledges financial support from Academy of Finland (grants 322085, 326291 and 329477). Johannes Kaarre is acknowledged for his contribution to the laboratory work.

Appendix A. Supplementary data

Supplementary data to this article can be found online at https://doi.org/10.1016/j.jclepro.2020.123020.

References

Abdel Gawwad, H.A., Abd El-Aleem, S., Ouda, A.S., 2016. Preparation and characterization of one-part non-Portland cement. Ceram. Int. 42, 220–228. https://doi.org/10.1016/j.ceramint.2015.08.096.

Adesanya, E., Ohenoja, K., Kinnunen, P., Illikainen, M., 2016. Alkali activation of ladle slag from steel-making process. J. Sustain.Metall. 1–11. https://doi.org/10.1007/s40831-016-0089-x.

Adesanya, E., Ohenoja, K., Luukkonen, T., Kinnunen, P., Illikainen, M., 2018a. One-part geopolymer cement from slag and pretreated paper sludge. J. Clean. Prod. 185, 168–175.

Adesanya, E., Ohenoja, K., Yliniemi, J., Illikainen, M., 2020. Mechanical transformation of phyllite mineralogy toward its use as alkali-activated binder precursor. Miner. Eng. 145, 106093. https://doi.org/10.1016/j.mineng.2019.106093.

Adesanya, E., Sreenivasan, H., Kantola, A.M., Telkki, V.-V., Ohenoja, K., Kinnunen, P., Illikainen, M., 2018b. Ladle slag cement – characterization of hydration and conversion. Construct. Build. Mater. 193, 128–134. https://doi.org/10.1016/j.conbuildmat.2018.10.179.

Belboom, S., Digneffe, J.-M., Renzoni, R., Germain, A., Léonard, A., 2013. Comparing technologies for municipal solid waste management using life cycle assessment methodology: a Belgian case study. Int. J. Life Cycle Assess. 18, 1513–1523. https://doi.org/10.1007/s11367-013-0603-3.

Ben Haha, M., Le Saout, G., Winnefeld, F., Lothenbach, B., 2011. Influence of activator type on hydration kinetics, hydrate assemblage and microstructural development of alkali activated blast-furnace slags. Cement Concr. Res. 41, 301–310. https://doi.org/10.1016/j.cemconres.2010.11.016.

Ben Haha, M., Lothenbach, B., Le Saout, G., Winnefeld, F., 2012. Influence of slag chemistry on the hydration of alkali-activated blast-furnace slag — Part II: effect of Al_2O_3. Cement Concr. Res. 42, 74–83. https://doi.org/10.1016/j.cemconres.2011.08.005.

Ben Haha, M., Lothenbach, B., Le Saout, G., Winnefeld, F., 2011. Influence of slag chemistry on the hydration of alkali-activated blast-furnace slag — Part I: effect of MgO. Cement Concr. Res. 41, 955–963. https://doi.org/10.1016/j.cemconres.2011.05.002.

Bernal, S.A., Provis, J.L., Fernández-Jiménez, Ana, Krivenko, Pavel, Kavalerova, Elena, Palacios, Marta, Shi, Caijun, 2014. Binder chemistry - high-calcium alkali-activated materials. In: Alkali Activated Materials - State-Of-The-Art Report RILEM TC 224-AAM. Springer, Dordrecht, pp. 59–91.

Bjørn, A., Owsianiak, M., Laurent, A., Olsen, S.I., Corona, A., Hauschild, M.Z., 2018. Scope definition. In: Hauschild, M.Z., Rosenbaum, R.K., Olsen, S.I. (Eds.), Life Cycle Assessment: Theory and Practice. Springer International Publishing, Cham, pp. 75–116. https://doi.org/10.1007/978-3-319-56475-3_8.

Carvalho, S.Z., Vernilli, F., Almeida, B., Demarco, M., Silva, S.N., 2017. The recycling effect of BOF slag in the portland cement properties. Resour. Conserv. Recycl. 127, 216–220. https://doi.org/10.1016/j.resconrec.2017.08.021.

Chavda, M.A., Bernal, S.A., Apperley, D.C., Kinoshita, H., Provis, J.L., 2015. Identification of the hydrate gel phases present in phosphate-modified calcium aluminate binders. Cement Concr. Res. 70, 21–28. https://doi.org/10.1016/j.cemconres.2015.01.007.

Chen, C., Habert, G., Bouzidi, Y., Jullien, A., 2010. Environmental impact of cement production: detail of the different processes and cement plant variability evaluation. J. Clean. Prod. 18, 478–485. https://doi.org/10.1016/j.jclepro.2009.12.014.

Collier, N.C., 2016. Transition and decomposition temperatures of cement phases – a collection of thermal analysis data. Ceramics - Silikaty 1–10. https://doi.org/10.13168/cs.2016.0050.

Cristelo, N., Fernández-Jiménez, A., Castro, F., Fernandes, L., Tavares, P., 2019. Sustainable alkaline activation of fly ash, aluminium anodising sludge and glass powder blends with a recycled alkaline cleaning solution. Construct. Build. Mater. 204, 609–620. https://doi.org/10.1016/j.conbuildmat.2019.01.226.

Di Maria, A., Salman, M., Dubois, M., Van Acker, K., 2018. Life cycle assessment to evaluate the environmental performance of new construction material from stainless steel slag. Int. J. Life Cycle Assess. 23, 2091–2109. https://doi.org/10.1007/s11367-018-1440-1.

Duxson, P., Fernández-Jiménez, A., Provis, J.L., Lukey, G.C., Palomo, A., van Deventer, J.S.J., 2007. Geopolymer technology: the current state of the art. J. Mater. Sci. 42, 2917–2933. https://doi.org/10.1007/s10853-006-0637-z.

En197-1, 2011. EN 197-1 Cement. Part 1: composition, quality requirements and conformity of common cements [WWW Document]. URL. https://online.sfs.fi/fi/index/tuotteet/SFS/CEN/ID2/1/182891.html.stx, 8.16.19.

Feng, Q., Yamamichi, H., Shoya, M., Sugita, S., 2004. Study on the pozzolanic properties of rice husk ash by hydrochloric acid pretreatment. Cement Concr. Res. 34, 521–526. https://doi.org/10.1016/j.cemconres.2003.09.005.

Fernández-Jiménez, A., Cristelo, N., Miranda, T., Palomo, Á., 2017. Sustainable alkali activated materials: precursor and activator derived from industrial wastes. J. Clean. Prod. 162, 1200–1209. https://doi.org/10.1016/j.jclepro.2017.06.151.

Garcia-Lodeiro, I., Palomo, A., Fernández-Jiménez, A., Macphee, D.E., 2011. Compatibility studies between N-A-S-H and C-A-S-H gels. Study in the ternary diagram Na2O–CaO–Al2O3–SiO2–H2O. Cement Concr. Res. 41, 923–931. https://doi.org/10.1016/j.cemconres.2011.05.006.

Gebregziabiher, B.S., Thomas, R., Peethamparan, S., 2015. Very early-age reaction kinetics and microstructural development in alkali-activated slag. Cement Concr. Compos. 55, 91–102. https://doi.org/10.1016/j.cemconcomp.2014.09.001.

Habert, G., 2013. A method for allocation according to the economic behaviour in the EU-ETS for by-products used in cement industry. Int. J. Life Cycle Assess. 18, 113–126. https://doi.org/10.1007/s11367-012-0464-1.

Habert, G., d'Espinose de Lacaillerie, J.B., Roussel, N., 2011. An environmental evaluation of geopolymer based concrete production: reviewing current research trends. J. Clean. Prod. 19, 1229–1238. https://doi.org/10.1016/j.jclepro.2011.03.012.

Humad, A.M., Kothari, A., Provis, J.L., Cwirzen, A., 2019. The effect of blast furnace slag/fly ash ratio on setting, strength, and shrinkage of alkali-activated pastes and concretes. Front. Mater. 6 https://doi.org/10.3389/fmats.2019.00009.

Ismail, I., Bernal, S.A., Provis, J.L., San Nicolas, R., Hamdan, S., van Deventer, J.S.J., 2014. Modification of phase evolution in alkali-activated blast furnace slag by the incorporation of fly ash. Cement Concr. Compos. 45, 125–135. https://doi.org/10.1016/j.cemconcomp.2013.09.006.

ISO 14040, 2006. ISO 14040:2006 - environmental management – Life cycle assessment – Principles and framework [WWW Document]. URL. https://www.iso.org/standard/37456.html, 6.26.17.

Lemougna, P.N., MacKenzie, K.J.D., Jameson, G.N.L., Rahier, H., Melo, U.F.C., 2013. The role of iron in the formation of inorganic polymers (geopolymers) from volcanic ash: a 57Fe Mössbauer spectroscopy study. J. Mater. Sci. 48, 5280–5286. https://doi.org/10.1007/s10853-013-7319-4.

Luukkonen, T., Abdollahnejad, Z., Yliniemi, J., Kinnunen, P., Illikainen, M., 2018a. One-part alkali-activated materials: a review. Cement Concr. Res. 103, 21–23. https://doi.org/10.1016/j.cemconres.2017.10.001.

Luukkonen, T., Abdollahnejad, Z., Yliniemi, J., Kinnunen, P., Illikainen, M., 2018b. Comparison of alkali and silica sources in one-part alkali-activated blast furnace slag mortar. J. Clean. Prod. 187, 171–179.

Maddalena, R., Roberts, J.J., Hamilton, A., 2018. Can Portland cement be replaced by low-carbon alternative materials? A study on the thermal properties and carbon emissions of innovative cements. J. Clean. Prod. 186, 933–942. https://doi.org/10.1016/j.jclepro.2018.02.138.

Majhi, R.K., Nayak, A.N., 2020. Production of sustainable concrete utilising high-volume blast furnace slag and recycled aggregate with lime activator. J. Clean. Prod. 255, 120188. https://doi.org/10.1016/j.jclepro.2020.120188.

Mallisa, H., Turuallo, G., 2017. The maximum percentage of fly ash to replace part of original Portland cement (OPC) in producing high strength concrete. AIP Conf. Proc. 1903, 030012 https://doi.org/10.1063/1.5011519.

Mellado, A., Catalán, C., Bouzón, N., Borrachero, M.V., Monzó, J.M., Payá, J., 2014. Carbon footprint of geopolymeric mortar: study of the contribution of the alkaline activating solution and assessment of an alternative route. RSC Adv. 4, 23846–23852. https://doi.org/10.1039/C4RA03375B.

Moraes, J.C.B., Font, A., Soriano, L., Akasaki, J.L., Tashima, M.M., Monzó, J., Borrachero, M.V., Payá, J., 2018. New use of sugar cane straw ash in alkali-activated materials: a silica source for the preparation of the alkaline activator. Construct. Build. Mater. 171, 611–621. https://doi.org/10.1016/j.conbuildmat.2018.03.230.

Newman, J., Choo, B.S., 2003. Advanced Concrete Technology 1: Constituent Materials, Chapter 2. Butterworth-Heinemann.
Nguyen, H., Adesanya, E., Ohenoja, K., Kriskova, L., Pontikes, Y., Kinnunen, P., Illikainen, M., 2019. Byproduct-based ettringite binder – a synergy between ladle slag and gypsum. Construct. Build. Mater. 197, 143–151. https://doi.org/10.1016/j.conbuildmat.2018.11.165.
Onisei, S., Douvalis, A.P., Malfliet, A., Peys, A., Pontikes, Y., 2018. Inorganic polymers made of fayalite slag: on the microstructure and behavior of Fe. J. Am. Ceram. Soc. 101, 2245–2257. https://doi.org/10.1111/jace.15420.
Osborne, G.J., 1999. Durability of Portland blast-furnace slag cement concrete. Cement Concr. Compos. 21, 11–21. https://doi.org/10.1016/S0958-9465(98)00032-8.
Papadakis, V.G., 2000. Effect of supplementary cementing materials on concrete resistance against carbonation and chloride ingress. Cement Concr. Res. 30, 291–299. https://doi.org/10.1016/S0008-8846(99)00249-5.
Passuello, A., Rodríguez, E.D., Hirt, E., Longhi, M., Bernal, S.A., Provis, J.L., Kirchheim, A.P., 2017. Evaluation of the potential improvement in the environmental footprint of geopolymers using waste-derived activators. J. Clean. Prod. 166, 680–689. https://doi.org/10.1016/j.jclepro.2017.08.007.
Peys, A., Rahier, H., Pontikes, Y., 2016. Potassium-rich biomass ashes as activators in metakaolin-based inorganic polymers. Appl. Clay Sci. 119, 401–409. https://doi.org/10.1016/j.clay.2015.11.003.
Pontikes, Y., Snellings, R., 2014. Chapter 16 - cementitious binders incorporating residues. In: Worrell, E., Reuter, M.A. (Eds.), Handbook of Recycling. Elsevier, Boston, pp. 219–229. https://doi.org/10.1016/B978-0-12-396459-5.00016-7.
Puertas, F., Torres-Carrasco, M., 2014. Use of glass waste as an activator in the preparation of alkali-activated slag. Mechanical strength and paste characterisation. Cement Concr. Res. 57, 95–104. https://doi.org/10.1016/j.cemconres.2013.12.005.
Puertas, F., Torres-Carrasco, M., Alonso, M.M., 2015. 4 - reuse of urban and industrial waste glass as a novel activator for alkali-activated slag cement pastes: a case study. In: Pacheco-Torgal, F., Labrincha, J.A., Leonelli, C., Palomo, A., Chindaprasirt, P. (Eds.), Handbook of Alkali-Activated Cements, Mortars and Concretes. Woodhead Publishing, Oxford, pp. 75–109.
Qu, B., Martin, A., Pastor, J.Y., Palomo, A., Fernández-Jiménez, A., 2016. Characterisation of pre-industrial hybrid cement and effect of pre-curing temperature. Cement Concr. Compos. 73, 281–288. https://doi.org/10.1016/j.cemconcomp.2016.07.019.
Rashad, A.M., Bai, Y., Basheer, P.A.M., Collier, N.C., Milestone, N.B., 2012. Chemical and mechanical stability of sodium sulfate activated slag after exposure to elevated temperature. Cement Concr. Res. 42, 333–343. https://doi.org/10.1016/j.cemconres.2011.10.007.
Rosenbaum, R.K., Hauschild, M.Z., Boulay, A.-M., Fantke, P., Laurent, A., Núñez, M., Vieira, M., 2018. Life cycle impact assessment. In: Hauschild, M.Z., Rosenbaum, R.K., Olsen, S.I. (Eds.), Life Cycle Assessment: Theory and Practice. Springer International Publishing, Cham, pp. 167–270. https://doi.org/10.1007/978-3-319-56475-3_10.
Salman, M., Dubois, M., Maria, A.D., Acker, K.V., Balen, K.V., 2016. Construction materials from stainless steel slags: technical aspects, environmental benefits, and economic opportunities. J. Ind. Ecol. 20, 854–866. https://doi.org/10.1111/jiec.12314.
Schrijvers, D.L., Loubet, P., Sonnemann, G., 2016. Developing a systematic framework for consistent allocation in LCA. Int. J. Life Cycle Assess. 21, 976–993. https://doi.org/10.1007/s11367-016-1063-3.
Scrivener, K.L., John, V.M., Gartner, E.M., 2018. Eco-efficient cements: potential economically viable solutions for a low-CO2 cement-based materials industry. Cement Concr. Res. 114, 2–26. https://doi.org/10.1016/j.cemconres.2018.03.015.
Shi, C., Day, R.L., 1995. A calorimetric study of early hydration of alkali-slag cements. Cement Concr. Res. 25, 1333–1346. https://doi.org/10.1016/0008-8846(95)00126-W.
Simon, S., Gluth, G.J.G., Peys, A., Onisei, S., Banerjee, D., Pontikes, Y., 2018. The fate of iron during the alkali-activation of synthetic (CaO-)FeOx-SiO2 slags: an Fe K-edge XANES study. J. Am. Ceram. Soc. 101, 2107–2118. https://doi.org/10.1111/jace.15354.
Sun, Z., Vollpracht, A., 2018. Isothermal calorimetry and in-situ XRD study of the NaOH activated fly ash, metakaolin and slag. Cement Concr. Res. 103, 110–122. https://doi.org/10.1016/j.cemconres.2017.10.004.
Suwan, T., Fan, M., 2017. Effect of manufacturing process on the mechanisms and mechanical properties of fly ash-based geopolymer in ambient curing temperature. Mater. Manuf. Process. 32, 461–467. https://doi.org/10.1080/10426914.2016.1198013.
Torres-Carrasco, M., Palomo, J.G., Puertas, F., 2014. Sodium silicate solutions from dissolution of glasswastes. Statistical analysis. Mater. Construcción 64, 14. https://doi.org/10.3989/mc.2014.05213.
Turner, L.K., Collins, F.G., 2013. Carbon dioxide equivalent (CO2-e) emissions: a comparison between geopolymer and OPC cement concrete. Construct. Build. Mater. 43, 125–130. https://doi.org/10.1016/j.conbuildmat.2013.01.023.
Van den Heede, P., De Belie, N., 2012. Environmental impact and life cycle assessment (LCA) of traditional and 'green' concretes: literature review and theoretical calculations. Cement Concr. Compos. 34, 431–442. https://doi.org/10.1016/j.cemconcomp.2012.01.004.
Van den Heede, P., De Belie, N., 2010. Durability related functional units for life cycle assessment of high-volume fly ash concrete. In: Second International Conference on Sustainable Construction Materials and Technologies, Proceedings. Presented at the Second International Conference on Sustainable Construction Materials and Technologies. UWM Center for By-Products Utilization, pp. 583–594.
van Deventer, J.S.J., Provis, J.L., Duxson, P., Brice, D.G., 2010. Chemical research and climate change as drivers in the commercial adoption of alkali activated materials. Waste and Biomass Valorization 1, 145–155.
van Riessen, A., Jamieson, E., Kealley, C.S., Hart, R.D., Williams, R.P., 2013. Bayer-geopolymers: an exploration of synergy between the alumina and geopolymer industries. Cement Concr. Compos. 41, 29–33. https://doi.org/10.1016/j.cemconcomp.2013.04.010.
Wang, J., Zhou, T., Xu, D., Zhou, Z., Du, P., Xie, N., Cheng, X., Liu, Y., 2018. Effect of nano-silica on the efflorescence of waste based alkali-activated inorganic binder. Construct. Build. Mater. 167, 381–390. https://doi.org/10.1016/j.conbuildmat.2018.02.006.
Zhang, P., Li, Q.-F., 2013. Durability of high performance concrete composites containing silica fume. Proc. IMechE 227, 343–349. https://doi.org/10.1177/1464420712460617.
Zhang, Z., Provis, J.L., Reid, A., Wang, H., 2014. Fly ash-based geopolymers: the relationship between composition, pore structure and efflorescence. Cement Concr. Res. 64, 30–41. https://doi.org/10.1016/j.cemconres.2014.06.004.
Zhang, Z., Wang, H., Provis, J.L., Reid, A., 2013. Efflorescence: a critical challenge for geopolymer applications? In: Dao, V., Dux, P. (Eds.), Concrete Institute of Australia's Biennial National Conference 2013. Presented at the Concrete Institute of Australia's Biennial National Conference (Concrete 2013): Understanding Concrete. Concrete Institute of Australia, Sydney, Australia, pp. 1–10.